Spontaneous Formation of One-Dimensional Hydrogen Gas Hydrate in Carbon Nanotubes

Wenhui Zhao,[†,#] Lu Wang,[†,#] Jaeil Bai,[‡,#] Joseph S. Francisco,*,[§] and Xiao Cheng Zeng*,[‡,†]

[†]Department of Materials Science and Engineering, University of Science and Technology of China, Hefei, Anhui 230026, China
[‡]Department of Chemistry, University of Nebraska—Lincoln, Lincoln, Nebraska 68588, United States,
[§]Department of Chemistry, Purdue University, West Lafayette, Indiana 47907, United States

Ⓢ *Supporting Information*

ABSTRACT: We present molecular dynamics simulation evidence of spontaneous formation of quasi-one-dimensional (Q1D) hydrogen gas hydrates within single-walled carbon nanotubes (SW-CNTs) of nanometer-sized diameter (1−1.3 nm) near ambient temperature. Contrary to conventional 3D gas hydrates in which the guest molecules are typically contained in individual and isolated cages in the host lattice, the guest H_2 molecules in the Q1D gas hydrates are contained within a 1D nanochannel in which the H_2 molecules form a molecule wire. In particular, we show that in the (15,0) zigzag SW-CNT, the hexagonal H_2 hydrate tends to form, with one H_2 molecule per hexagonal prism, while in the (16,0) zigzag SW-CNT, the heptagonal H_2 hydrate tends to form, with one H_2 molecule per heptagonal prism. In contrast, in the (17,0) zigzag SW-CNT, the octagonal H_2 hydrate can form, with either one H_2 or two H_2 molecules per pentagonal prism (single or double occupancy). Interestingly, in the hexagonal or heptagonal ice nanotube, the H_2 wire is *solid-like* as the axial diffusion constant is very low (<5 × 10^{-10} cm^2/s), whereas in the octagonal ice nanotube, the H_2 wire is *liquid-like* as its axial diffusion constant is comparable to 10^{-5} cm^2/s.

Ice Nanotube   Q1D H₂ hydrate
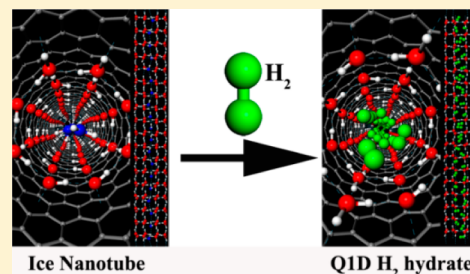
INTRODUCTION

Gas hydrates belong to a class of host−guest compounds. The host is typically a lattice of water that contains independent cages in which each cage can accommodate one or a few guest molecules, depending on the size of the guest molecule and diameter of the cages.[1] To date, three crystalline structures of 3D gas hydrates have been uncovered, namely, type I, II, and H clathrate structures. Gas hydrates have attracted considerable interests because of their significant energy and environmental implications. In nature, methane hydrates in type I structure are predominantly present at ocean floor and polar region, while gas hydrates with type II or H structure are found in the Gulf of Mexico.[2] On the negative side, during the deepwater−oil/gas production, plugging of pipelines by gas hydrates may cause environment hazards.

Besides being as natural gas reserves, gas hydrates have also been exploited for potential applications as gas-storage media, such as for storing CO_2 (e.g., for carbon sequestration) or hydrogen (an energy carrier).[3−9] For a long time, hydrogen molecules were thought too small to be capable of stabilizing the host lattice of ice clathrates. However, in 2002, Mao et al. revealed that H_2 hydrates can be stable at high pressures (>200 MPa) and room temperature in which H_2 molecules can occupy both the small and large cages in the type II crystalline structure.[3] This finding has prompted subsequent efforts in synthesizing gas hydrates as potential media for hydrogen storage. For example, to achieve the formation of H_2 hydrates at near-ambient condition, various promoter molecules such as tetrahydrofurn (THF) have been examined.[10−13] These

previous studies indicate that water cages may offer a safe and clean way to store hydrogen.

To date, structural and thermodynamic properties of several 3D H_2 hydrates have been well characterized.[14−20] However, the formation mechanism of bulk H_2 hydrates remains less understood due in part to the inability to precisely monitoring the time frame and spatial domain of the crystallization process in the laboratory, or due to very long computing time needed in molecular dynamics simulations of bulk gas hydrate formation.[21] On the other hand, highly confined environment not only can disrupt the hydrogen-bonding network of ice framework thereby affecting kinetics of crystallization, but also allow spontaneous formation of some low-dimensional ice structures at nanosecond time scale.[22−30] Indeed, spontaneous formation of low-dimensional gas hydrates (e.g., argon and methane hydrates), as well as guest-free hydrates, was observed in previous molecular dynamics simulations.[29−31] Previous simulation and experimental studies have also shown that water molecules can enter into single-walled carbon nanotubes (SW-CNTs) without applying high hydrostatic pressure.[32−35] Liquid water inside a SW-CNT can diffuse along the axial direction at room temperature (with typical diffusion constant D of ∼10^{-5} cm^2 s^{-1}), while far below the room temperature, the axial diffusion constant of quasi-one-dimensional (Q1D) solid water, e.g., ice nanotubes, is about 10^{-10} cm^2 s^{-1}.[33,36] It is known that ice nanotubes consist of polygonal water prisms. Can the
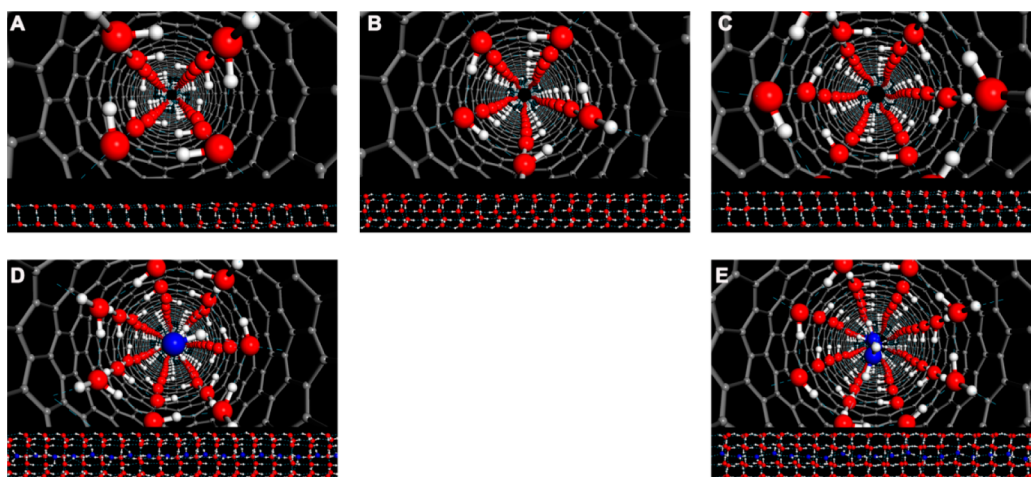
Figure 1. Axial views (top panels) and side views (bottom panels) of the inherent structures of single-walled ice nanotubes (INTs): (A) hollow tetragonal INT formed in (13, 0) SW-CNT; (B) hollow pentagonal INT formed in (14, 0) SW-CNT; (C) hollow hexagonal INT formed in (15, 0) SW-CNT; (D) core−sheath heptagonal INT formed in (16, 0) SW-CNT; (E) core−sheath octagonal INT formed in (17, 0) SW-CNT. Red, white, and gray spheres represent oxygen, hydrogen, and carbon atoms, respectively. Light blue dotted lines denote hydrogen bonds. Blue spheres in (D) and (E) represent oxygen atoms in water wire encapsulated inside the heptagonal and octagonal INTs.

polygonal water prisms trap one or more H_2 molecules to form H_2 clathrate structures? Here, we show simulation evidence of spontaneous formations of Q1D H_2 hydrates inside SW-CNTs of nanometer-sized diameter. Stability of the predicted H_2 hydrate structures are further confirmed by density-functional theory optimization and ab initio molecular dynamics simulations.

■ COMPUTATIONAL METHODS

Classical Molecular Dynamics Simulations. Independent MD simulations are performed using the Gromacs 4.5 software package for water encapsulated in SW-CNT systems.[37] Five zigzag SW-CNTs with index (13, 0), (14, 0), (15, 0), (16, 0), and (17,0) are considered. Here, carbon atoms are modeled as uncharged Lennard-Jones (LJ) particles with graphite parameters of $\varepsilon_C = 0.2328$ kJ/mol and $\sigma_C = 0.34$ nm.[38] TIP3P model of water are used in most MD simulations,[39] while several other three-site, four-site, and five-site water models (SPC, SPC/E, TIP4P, and TIP5P) are also examined for test simulations which give the same qualitative results of the Q1D H_2 hydrate formation as with the TIP3P water model. H_2 molecules are described by a rigid two-center LJ model with a bond length of 0.074 nm and with the LJ parameters of $\varepsilon_H = 0.1039$ kJ/mol and $\sigma_H = 0.259$ nm.[40] LJ potential parameters for heterogeneous atoms are given by Lorentz−Berthelot rule. In addition to the LJ potential for H_2, more accurate exp-6-8-10 potentials for the H_2−H_2 and H_2−C interactions[41−43] are also considered. A test simulation shows that the results of Q1D H_2 hydrate formation are very close to those obtained based on the LJ potential (see Figure S1 in Supporting Information), indicating that the H_2 hydrate formation is not very sensitive to the selected H_2 and H_2−C potentials (developed by different groups). The cutoff length for all interparticle interactions is set to be 2.0 nm. The periodic boundary condition is applied in all three dimensions. In the axial direction, the supercell (or CNT) has a fixed length of 5.112 nm. Such a fixed length of CNT is selected based on our previous MD simulations of the formation of polygonal ice nanotube within CNTs.[36] Test simulations show that the CNTs can accommodate 18 layers of polygonal water rings, i.e., one layer per 0.284 nm, close to the typical distance of a hydrogen-bonding pair of oxygen atoms. In the two lateral directions, the supercell lengths are 5.0 nm, respectively, which are large enough to neglect interaction among periodic images. The temperature is controlled by using the velocity-scaling method.[44]

Density-Functional Theory Calculations and ab Initio Molecular Dynamics Simulations. Density functional theory (DFT) calculations and ab initio MD (AIMD) simulations are performed by using QUICKSTEP module implemented in the CP2K package.[45] Molecules are described with the hybrid Gaussian and plane-wave method. The ion-valence electron interactions are represented by norm-conserving pseudopotentials developed by Goedecker and co-workers,[46,47] and the charge density cutoff of 280 Ry is used for the auxiliary basis set. The BLYP[48,49] exchange-correlation functional is used together with Grimme dispersion correction (D3).[50] We select the BLYP-D3 functional because it can properly describe systems with weak hydrogen-bonding interactions.[51−53] A previous AIMD simulation study using BLYP-D3 also showed good agreement between the theoretical and experimental results of the electronic absorption spectrum of liquid water.[54] In addition to the BLYP-D3 functional, the Perdew−Burke−Ernzerhof (PBE) exchange-correlation functional[55] with Grimme dispersion correction (D3)[50] is also considered for geometric optimization. Nearly the same optimized geometric structures are obtained as those based on the BLYP-D3 functional.

Kohn−Sham orbitals are expanded into a double-ζ valence polarized basis set (DZVP). We adopt a strict convergence criterion for the electronic gradient 1×10^{-7} eV with the orbital transformation method. A tetragonal supercell $(50 \times 50 \times 8.52$ Å$)$ is undertaken for all the structures with the axis of the CNT being along the z-direction. Convergence criterion for the maximum force is set to 0.01 eV/Å in all the geometry optimizations. Vibrational analysis is carried out to examine dynamic stability of the optimized periodic structures. No imaginary frequencies are found from the vibrational analysis, suggesting the optimized structures are local energy minima. Basis set superposition error (BSSE) is corrected to obtain the interaction energy E_i between a hydrogen molecule and inner surface of the ice nanotubes (enclosed in a SW-CNT), which is defined as $E_i = E(A + B) - E(A) - E(B)$, where $E(A + B)$ represents the total energy of the whole system, $E(A)$ and $E(B)$ represent the BSSE-corrected total energies of the (A) hydrogen molecules and (B) an ice nanotube enclosed in the SW-CNT. For Born−Oppenheimer AIMD simulations, all the AIMD trajectories (10 ps for each system) are generated in the constant volume and constant temperature ensemble, with the Nóse-Hoover chain method used for controlling the temperature (fixed at 250 K). The length of SW-CNT is always fixed at 0.852 nm. The time step of 1.0 fs is used, which has been proven to yield sufficient energy conservation for water systems.[52−54]

■ RESULTS AND DISCUSSION

The first series of classical MD simulations involve five SW-CNT/water systems to identify candidate ice-nanotube structures below the freezing point. The five zigzag SW-CNTs with the indexes (13, 0), (14, 0), (15, 0), (16, 0), and (17, 0) have the diameter of 10.18, 10.96, 11.74, 12.53, and 13.31 Å, respectively. On the basis of previous MD simulation results,[36] we place $18 \times n$ (n = 4, 5, or 6) water molecules in the three narrower SW-CNTs, respectively, and $18 \times (n + 1)$ (n = 7 or 8) in the two wider SW-CNTs to form perfect Q1D ice nanotubes. Different numbers of water molecules are also tested, and the spontaneous formation of ice nanotube structures (with some defects) is still observed (see Figure S2). All the five CNT/water systems are initially equilibrated at T = 1000 K and then subjected to an instant quench to T = 250 K. After 20 ns equilibration, the hollow single-walled tetragonal, pentagonal and hexagonal ice nanotubes are formed in the (13, 0), (14, 0) and (15, 0) SW-CNTs, respectively, whereas the core−sheath heptagonal and octagonal ice nanotubes with a 1D water wire in the interior region are observed in the (16, 0) and (17, 0) SW-CNTs (see Figure 1).

Clearly, to form Q1D hydrogen hydrates in these CNT/water systems, the H_2 molecules have to either occupy the hollow space within narrower ice nanotubes or displace the interior water wire within the core−sheath ice-nanotubes. Our second series of MD simulations are aimed to examine these possibilities. We initially place various mixtures of water and H_2 molecules within the five SW-CNTs and run the MD simulations to let the systems reach equilibrium at T = 1000 K. Next, the systems are subjected to an instant quench to T = 250 K, following by another 20 ns MD simulations. Results after 20 ns equilibration are summarized below:

(1) In the (13, 0) SW-CNT system, the supercell initially contains 72 ($18 \times n$, n = 4) water molecules and 18 H_2 molecules (i.e., H_2O/H_2 ratio is 4:1). During the 20 ns equilibration run at 250 K, a pentagonal composite ice nanotube is formed spontaneously, where some H_2 molecules occupy the wall of the ice nanotube rather than the hollow space (see Figure 2A). When the number of water molecules is reduced from 72 to 54 (H_2O/H_2 ratio 3:1), phase-separated structures, i.e., a tetragonal ice nanotube together with a high-density H_2 gas, are observed (see Figure 2B). Despite of repeated cooling/heating and long-time simulation, the Q1D tetragonal H_2 hydrate is not observed in the (13, 0) SW-CNT.

In addition, an independent AIMD starting with a perfect Q1D tetragonal H_2 hydrate (with 12 water molecules and 3 H_2 molecules) is performed. As shown in Supporting Information Movie S1, the AIMD trajectory of H_2 molecules in the tetragonal ice nanotube confirms that the 1D tetragonal H_2 hydrate is unstable in the (13, 0) SW-CNT. We also compute the interaction energy between a H_2 and the inner wall of tetragonal ice nanotube based on a DFT method with inclusion of BSSE correction and dispersion correction. The positive interaction energy (0.5 eV) indicates that the interaction is repulsive. Hence, both the AIMD simulation and DFT calculation show that 1D tetragonal H_2 hydrate cannot form within the (13, 0) SW-CNT. In other words, H_2 molecules cannot occupy the interior space of a tetragonal ice nanotube.

(2) In the (14, 0) SW-CNT system, the numbers of water molecules and H_2 molecules are chosen to be 90 ($18 \times n$, n = 5) and 18 (i.e., H_2O/H_2 ratio is 5:1). Spontaneous formation of the pentagonal H_2 hydrate (Movie S2) is observed. The ice
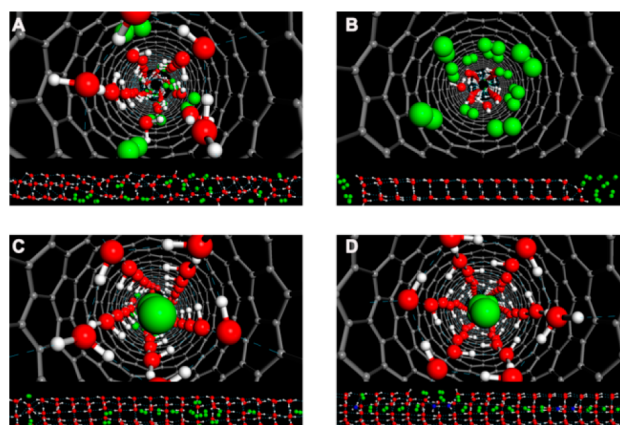

Figure 2. Axial views (top panels) and side views (bottom panels) of the inherent structures of binary mixtures of water and H_2 molecules. The inherent structures are generated from the final snapshot of independent classical MD simulations at 250 K. (A) Pentagonal-like composite ice nanotube formed in (13, 0) SW-CNT (H_2O/H_2 ratio 4:1); (B) phase-separated INT and H_2 gas in (13, 0) SW-CNT (H_2O/H_2 ratio 3:1); (C) pentagonal H_2 hydrate formed in (14, 0) SW-CNT (H_2O/H_2 ratio 5:1); (D) hexagonal H_2 hydrate formed in (15, 0) SW-CNT (H_2O/H_2 ratio 6:1). Green spheres represent H_2 molecules. Blue spheres represent oxygen atoms of H_2O molecules in the core region.

framework of pentagonal H_2 hydrate is identical to that of the pentagonal ice nanotube (other than a few defects). In other words, H_2 molecules can be enclosed in the interior nanochannel of the pentagonal ice nanotube (see Figure 2C). Moreover, we can obtain a nearly perfect pentagonal H_2 hydrate via repeated cooling/heating, followed by longer simulation and tuning the numbers of water molecules and H_2 molecules. An independent AIMD trajectory starting with a perfect pentagonal H_2 hydrate (containing 15 water molecules and 3 H_2 molecules) shows that the pentagonal H_2 hydrate is stable in the (14,0) SW-CNT (Movie S3). However, the computed BSSE-corrected interaction energy between the H_2 molecule and pentagonal ice nanotube is about 0.1 eV. This positive binding energy indicates that H_2 molecules may be easily released from the pentagonal H_2 hydrate if the CNT system is an open-end system. Higher pressures are needed to trap H_2 molecules within the pentagonal ice nanotube.

(3) In the (15, 0) SW-CNT system, the numbers of water molecules and H_2 molecules are chosen to be 108 ($18 \times n$, n = 6) and 18 (i.e., H_2O/H_2 ratio is 6:1). Spontaneous formation of a nearly perfect hexagonal H_2 hydrate (Movie S4) is observed. Like Q1D pentagonal H_2 hydrate, the H_2 molecules are enclosed in the interior nanochannel of the hexagonal ice nanotube (see Figure 2D). Within the hexagonal ice nanotube, each hexagonal prism is singly occupied by a H_2 molecule. Thus, the molecular ratio between number of H_2 molecules and water molecules is 1:6. Contrary to the 1D pentagonal H_2 hydrate, the BSSE-corrected interaction energy between H_2 molecule and hexagonal ice nanotube is about −0.09 eV, suggesting that it is energetically favorable for H_2 molecules to be trapped inside the hexagonal ice nanotube. Furthermore, an independent AIMD trajectory starting with a perfect hexagonal H_2 hydrate (containing 18 water molecules and 3 H_2 molecules) shows that the hexagonal H_2 hydrate is stable in the (15, 0) SW-CNT at 250 K (Movie S5).

(4) In the (16, 0) SW-CNT system, the numbers of 126 ($18 \times n$, n = 7) water molecules and 18 H_2 molecules are chosen

(i.e., H_2O/H_2 ratio is 7:1). After 20 ns equilibration at 250 K, a heptagonal H_2 hydrate with some defects is observed, as shown in Figure 3A (also see Movie S6). Here, the original interior
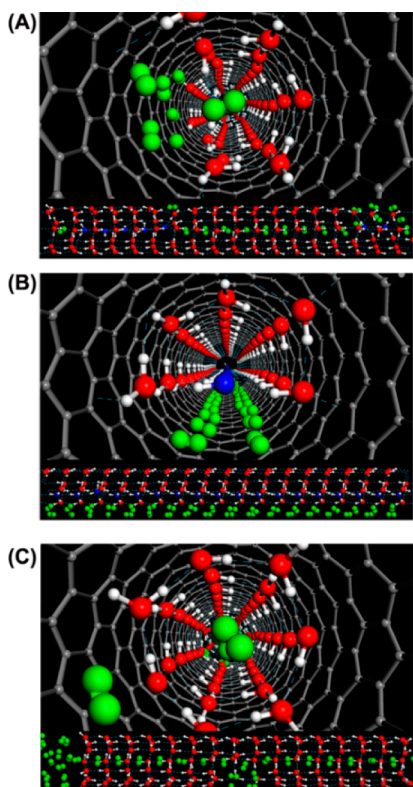

Figure 3. Axial views (top panels) and side views (bottom panels) of the inherent structures of the Q1D H_2 hydrates formed in (16, 0) SW-CNT. The inherent structures are generated from the final snapshot of independent classical MD simulations at 250 K (or 280 K). (A) Heptagonal H_2 hydrate (H_2O/H_2 ratio 7:1); (B) a composite ice/H_2 nanotube structure (H_2O/H_2 ratio 3:1); (C) a heptagonal H_2 hydrate together with a phase-separated H_2 gas (from snapshot of classical MD at 280 K) (H_2O/H_2 ratio 3:1).

water wire inside the core/sheath heptagonal ice nanotube is now replaced by the H_2 wire. Within the heptagonal H_2 hydrate each heptagonal prism contains a single H_2 molecule. Since the interior space of the heptagonal prism is larger than of the hexagonal prism, one may ask the question whether each heptagonal prism could be doubly occupied by two H_2 molecules. To explore this possibility, we reduce the number of water molecules to 108 and increase the number of H_2 molecules to 36 (i.e., H_2O/H_2 ratio is 3:1). After 20 ns equilibration at 250 K (starting from an initial configuration obtained at 1000 K), a composite ice/H_2 nanotube structure is observed, where the H_2 molecules replace two neighboring water chains on the wall of the core/sheath heptagonal ice nanotube, as shown in Figure 3B (also see Movie S7). By heating the composite ice/H_2 nanotube system in three steps to 280 K (20 ns per step), the heptagonal ice hydrate is formed where some H_2 molecules are encapsulated in the interior nanochannel of the heptagonal ice nanotube, indicating the composite ice/H_2 nanotube is a metastable structure. However, the occupancy of each heptagonal prism is still one, as shown in Figure 3C (also see Movie S8), indicating that the singly occupied heptagonal H_2 hydrate is thermodynamically more favorable.

Although the doubly occupancy for the heptagonal H_2 hydrate is not observed in the MD simulation, the AIMD trajectories starting with a perfect heptagonal H_2 hydrate (containing 21 water molecules and 3 or 6 H_2 molecules) suggest that 1D heptagonal H_2 hydrates with either single or double occupancy per heptagon prism are stable in the (16, 0) SW-CNT (see Movies S9 and S10). The computed BSSE-corrected interaction energy between the first H_2 molecule and heptagonal ice nanotube of the doubly occupied heptagonal H_2 hydrates is about −0.12 eV. However, the interaction energy between the second H_2 molecule and ice nanotube is positive, suggesting that the doubly occupancy is energetically unfavorable.

(5) Lastly, in the (17, 0) SW-CNT system, the numbers of water and H_2 molecules are chosen to be 144 ($18 \times n$, $n = 8$) and 18 (i.e., H_2O/H_2 ratio is 8:1). After 20 ns equilibration at 250 K, a nearly perfect singly occupied octagonal H_2 hydrate is formed spontaneously, as shown in Figure 4A (also see Movie S11). To examine possibility of the double occupancy for the octagonal H_2 hydrate, we increase the number of H_2 molecules to 27 (i.e., H_2O/H_2 ratio is 16:3). Interestingly, spontaneous formation of a nearly perfect octagonal H_2 hydrate at 250 K with both single and double occupancy is observed, as shown in Figure 4B (also see Movie S12). Furthermore, when the number of H_2 molecules is increased to 36 (i.e., H_2O/H_2 ratio is 4:1), a full doubly occupied octagonal H_2 hydrate with some defects is formed at 250 K (see Figure 4C and Movie S13). Subsequent simulations by increasing the temperature to 260 K for 20 ns, 270 K for 20 ns and then to 280 K for 20 ns also yield a nearly perfect octagonal H_2 hydrate with double occupancy per octagonal prism (see Figure 4D and Movie S14). In addition, the computed BSSE-corrected interaction energy between the H_2 molecules and octagonal ice nanotube is about −0.05 eV. Thus, the octagonal H_2 hydrate with double occupancy per octagonal prism is also energetically favorable. AIMD trajectories starting with a perfect octagonal H_2 hydrate (containing 24 water molecules and 3 or 6 H_2 molecules) also show that the octagonal H_2 hydrates with either single or double occupancy per octagon prism in the (17, 0) SW-CNT are stable at 250 K (see Movies S15 and S16). Hence, H_2 molecules can stabilize the octagonal ice nanotube to form Q1D H_2 hydrates through either single or double occupancy, for which the molecular ratio of H_2 molecules and water molecules ranges from 1:8 to 1:4.

Both the classical and ab initio MD simulations demonstrate that the n-gonal H_2 hydrates ($n = 5-8$) can be formed in corresponding (14,0), (15,0), (16,0), and (17,0) SW-CNTs. The SW-CNTs with a supercell length of 5.112 nm can accommodate 18 n-gonal prisms with each prism hosting at least one H_2 molecule (an octagonal prism can host two H_2 molecules). Thus, to achieve perfect n-gonal H_2 hydrate structures, we place $18 \times n$ water and 18 H_2 molecules initially in the supercell. If the number of water and H_2 molecules does not follow the ideal ratio, some defects would be created in the n-gonal H_2 hydrate (see Figure S3). Moreover, Figure S3 shows that slightly excessive water molecules in the supercell will block the formation of a perfect H_2 chain in the hydrate since the extra water tend to occupy the center of hydrate, whereas insufficient number of the water molecules in the supercell will tend to induce some vacancies in the ice-nanotubes. Alternatively, with slightly deficient number of water molecules from the ideal H_2O/H_2 ratio (i.e., H_2O/H_2 ratio <8:1), a mixed 8-/7-gonal Q1D H_2 hydrate is formed in (17,0) SW-CNT (see
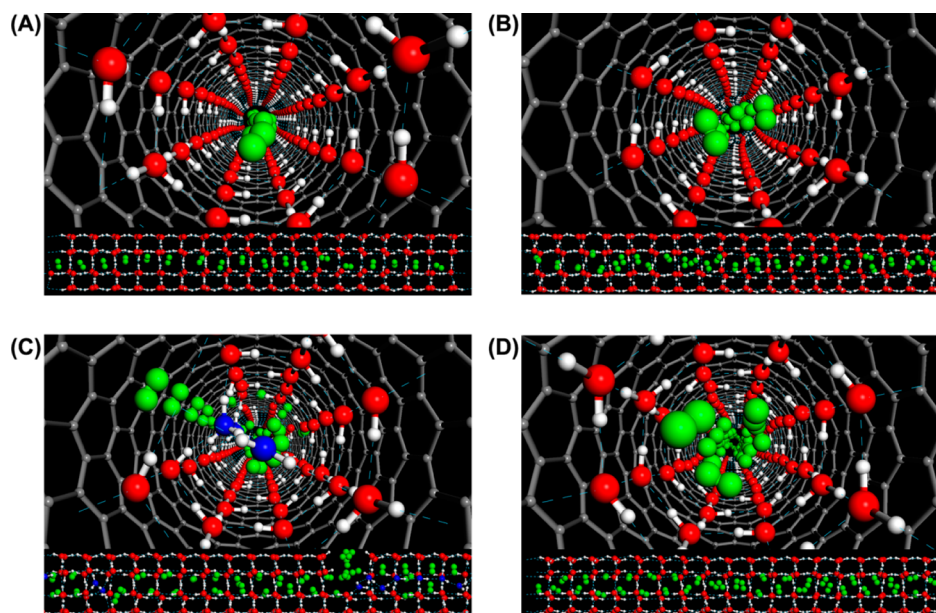
Figure 4. Axial views (top panels) and side views (bottom panels) of the inherent structures of the Q1D octagonal H_2 hydrates formed in (17, 0) SW-CNT. The inherent structures are generated from the final snapshot of independent classical MD simulations at 250 K (or 280 K). (A) Singly occupied (per prism) octagonal H_2 hydrate (H_2O/H_2 ratio 8:1); (B) a nearly perfect octagonal H2 hydrate with both single and double occupancy (H_2O/H_2 ratio 16:3); (C) doubly occupied (per prism) octagonal H_2 hydrate with some defects (H_2O/H_2 ratio 4:1); (D) a nearly perfect doubly occupied octagonal H_2 hydrate (from snapshot of MD at 280 K) (H_2O/H_2 ratio 4:1).

Figure S3A) rather than the 8-gonal Q1D H_2 hydrate. If N_w = 18 × 7 and N_{H2} = 18 (i.e., H_2O/H_2 ratio =7:1), the hydrate ends up to a 7-gonal Q1D hydrate. Likewise, with slightly deficient number of water molecules (i.e., H_2O/H_2 ratio <7:1), a mixed 7-/6-gonal H_2 hydrate is formed in the (16,0) SW-CNT, and if N_w = 18 × 6, i.e., H_2O/H_2 ratio = 6:1, the 6-gonal hydrate is formed (see Figure S3B). In stark contrast, with (15,0) SW-CNT and slightly deficient number of water molecules (i.e., H_2O/H_2 ratio <6:1), a perfect 6-gonal H_2 hydrate and a phase-separated H_2 gas are formed, rather than a mixed 6-/5-gonal H_2 hydrate (see Figure S3C).

In Table 1, we summarize structures of the Q1D H_2 hydrates, together with corresponding H_2O/H_2 ratio, occupancy of H_2 in every polygonal prism, hydrogen weight percentage (wt %), and the collapse temperature ($T_{collapse}$) of the hydrates. The result that $T_{collapse}$ of the pentagonal hydrate is much lower than that of other Q1D hydrates suggests that H_2 molecules can be easily released from the pentagonal H_2, consistent with the computed BSSE-corrected interaction energy. Also, $T_{collapse}$ of doubly occupied octagonal hydrate is much higher than that of singly and/or mixed singly/doubly occupied octagonal hydrate, indicating the octagonal hydrate with double occupancy is the most stable.

To gain more insight into the structural features of these polygonal ice nanotubes and H_2 hydrates, we compute the radial and axial density profiles, as shown in Figures 5, 6 and S4. The radial density profiles confirm that the tetragonal, pentagonal and hexagonal ice nanotubes are hollow, while the heptagonal and octagonal ice nanotubes are core−sheath, i.e., containing a water wire in the interior nanochannel (Figure 5A). Figure 5B−F shows that all ice nanotubes exhibit periodically layered structures in the axial direction. Interestingly, it can be seen from Figure 5E,F that the heptagonal and octagonal ice nanotubes exhibit notably different density distribution in the axial direction, even though both ice nanotubes encapsulate a water wire. For the heptagonal core−

Table 1. Structures of Q1D H_2 Hydrates, H_2O/H_2 Molecular Ratio, Occupancies of H_2 per Polygonal Prism, Hydrogen Weight Percentage (wt %), and the Collapse Temperature of Hydrates

SW-CNTs	H_2 hydrate	H_2O/H_2 ratio	occupancy	wt % of H_2	$T_{collapse}$ (K)[a]
(14,0)	5-gonal	5:1	single	0.37	290
(15,0)	6-gonal	6:1	single	0.34	390
	phase-separated	<6:1			
(16,0)	7-gonal	7:1	single	0.32	400
	Mixed 7-gonal/6-gonal	(6:1, 7:1)	single	(0.32, 0.33)	
	6-gonal	6:1	single	0.33	300
(17,0)	7-gonal	7:1	single	0.30	330
	Mixed 8-gonal/7-gonal	(7:1, 8:1)	single	(0.29, 0.30)	
	8-gonal	8:1	single	0.29	330
		(8:1, 8:2)	single/double	(0.29, 0.58)	
		8:2	double	0.58	410

[a]$T_{collapse}$ is the temperature at which 50% clathrate cages are collapsed, computed by heating the clathrates from 250 in 10 K temperature step (20 ns per temperature step). The initial configurations are the perfect hydrate structures to ignore effects of defects.

sheath nanotube, there is a low peak between every two neighboring high peaks and the density values at valleys are always close to 0, suggesting that the water molecules in the water wire are entrapped in the center of each heptagonal prism and their migration rate is very slow (the axial diffusion constant is 3×10^{-10} cm²/s). As such, the water wire is solid-like. However, for the octagonal core−sheath nanotube, no low peak is seen between every two neighboring high peaks and the valley values are still appreciable, suggesting that water
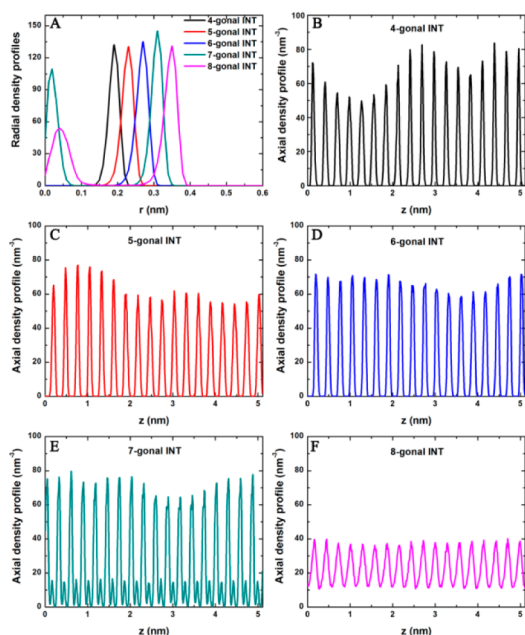
Figure 5. (A) Radial density profiles of polygonal INTs. Axial density profiles of (B) tetragonal, (C) pentagonal, (D), hexagonal, (E) heptagonal, and (F) octagonal INTs.
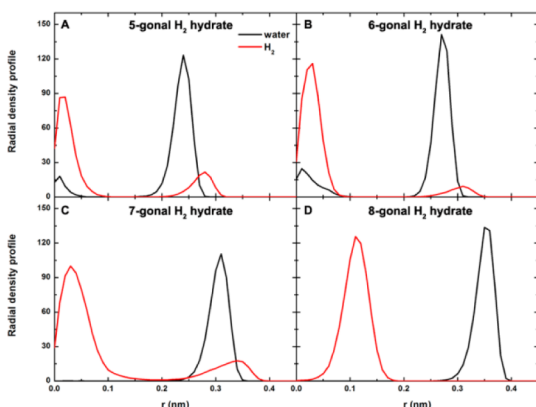

Figure 6. Radial density profiles of (A) pentagonal, (B), hexagonal, (C) heptagonal, and (D) octagonal H_2 hydrates.

molecules in the water wire can pass through each octagonal water rings easily (the axial diffusion constant is 1×10^{-6} cm^2/s). Hence, the water wire is liquid-like, consistent with the experimental result of "*nanotube water*".[56]

The radial density profiles of polygonal H_2 hydrates confirm that H_2 molecules are trapped in the interior nanochannel of corresponding polygonal ice nanotubes. As the diameter of SW-CNT increases, the trapped H_2 molecules tend to be located off the center (see Figure 6). Figure S4 shows a common feature for all polygonal H_2 hydrates, that is, each density peak of H_2 appears between neighboring water density peaks, indicating that H_2 molecules prefer to be located at the center of each polygonal prism. However, there is a notable distinction between octagonal H_2 hydrate and other ones, namely, the density distributions of H_2 are still appreciable even at center of the water octagonal rings whereas those in other polygonal H_2 hydrates are nearly zero. This means that the probability of H_2 molecules located at water ring is very small in heptagonal or narrower H_2 hydrates (even though the AIMD trajectory shows that H_2 molecules in heptagonal H_2 hydrate can easily pass

through the heptagonal rings (see Movie S9)), but the probability is much larger in octagonal ice nanotube. Therefore, the rate of H_2 migration through octagonal rings can be much higher than that in the H_2 hydrates with smaller diameter. Indeed, the axial diffusion constant of H_2 in octagonal hydrates is about 1×10^{-5} cm^2/s (liquid-like, Figure 7D–F), whereas those in narrower hydrates are less than 5×10^{-10} cm^2/s (250 K, Figure 7A–C). With increasing temperature, the axial diffusion constants of H_2 molecules are of the same magnitude as those of water in pentagonal and hexagonal hydrates below the collapse temperature, suggesting that H_2 molecule can hardly pass through the pentagonal and hexagonal water rings (Figure 7A,B). It can be also seen from Figure 7C that the H_2 axial diffusion constant is about an order of magnitude greater than that of water in heptagonal clathrate at 390 K, indicating that H_2 molecule can pass through the heptagonal water rings.

Note that the H_2 diffusivity within a hydrate having defects is dependent on the type of defects. For example, the axial diffusion constant of H_2 in a metastable composite ice/H_2 hexagonal nanotube in (16, 0) SW-CNT at 250 K is about 7×10^{-6} cm^2/s, suggesting the H_2 molecules in the composite ice/H_2 nanotube can move more freely along the axial direction (Figure 3B). When the heptagonal ice hydrate is formed by heating the composite ice/H_2 nanotube to 280 K (Figure 3C), the axial diffusion constant of H_2 is reduced to about 8×10^{-8} cm^2/s, about 2 orders of magnitude lower. In this case, the heptagonal water rings can block diffusion of H_2 molecules in the axial direction.

Finally, we perform additional classical MD simulations to demonstrate that the Q1D H_2 clathrates can be also formed spontaneously near ambient pressure. Toward this end, we first place a finite-size SW-CNT into a dilute H_2 aqueous solution. The solution is initially equilibrated at 300 K and 1 atm, followed by stepwise cooling in a temperature step of 10 K (see the Supporting Information for computational details). At 250 K, the spontaneous formation of heptagonal H_2 hydrates is observed in (17,0) SW-CNT (Figure 8A and Movies S17), while octagonal H_2 hydrate is formed spontaneously in (18,0) SW-CNT at 220 K (see Figure 8B and Movies S18).

■ CONCLUSION

We have shown that polygonal ice nanotubes and Q1D H_2 hydrates can be formed spontaneously inside SW-CNTs of nanometer-size diameter near ambient temperature. In relatively wider SW-CNT, e.g., (16,0) and (17,0), the Q1D H_2 hydrates exhibit core−sheath structures, i.e., H_2 molecules occupy the interior core (by replacing the original interior water wire) of the either heptagonal or octagonal ice nanotubes, forming a H_2 wire. Notably, in the octagonal ice nanotube, liquid-like transport of H_2 molecules in the axial direction can be observed. In the relatively narrow SW-CNT, e.g, (15,0), the Q1D hydrate also exhibits the core−sheath structure with H_2 molecules occupying the interior core of the hexagonal ice nanotube, forming a solid-like H_2 wire. Further DFT calculations indicate that the interaction energy between a H_2 and the inner wall of these ice nanotubes is attractive and thus energetically favorable at single occupancy. Ab initio molecular dynamics simulation suggests that these H_2 hydrates are stable at 250 K within the SW-CNTs. Unlike conventional bulk gas hydrates (with type I, II or H structure) where the guest molecules are typically contained in isolated cages in the ice framework, the H_2 molecules in the Q1D gas hydrates are contained within a 1D nanochannel and form a either solid-like
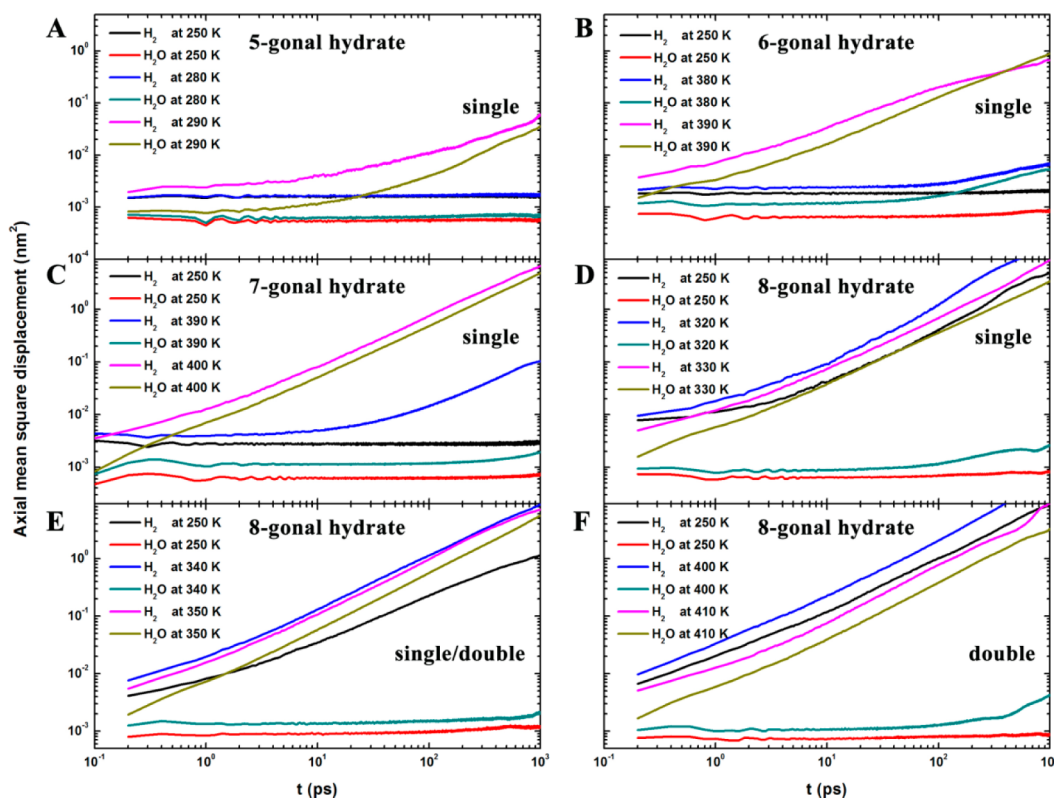
Figure 7. Calculated mean square displacement (MSD) in the axial direction for H_2 and water molecules in the center of Q1D H_2 hydrates (formed in SW-CNTs).
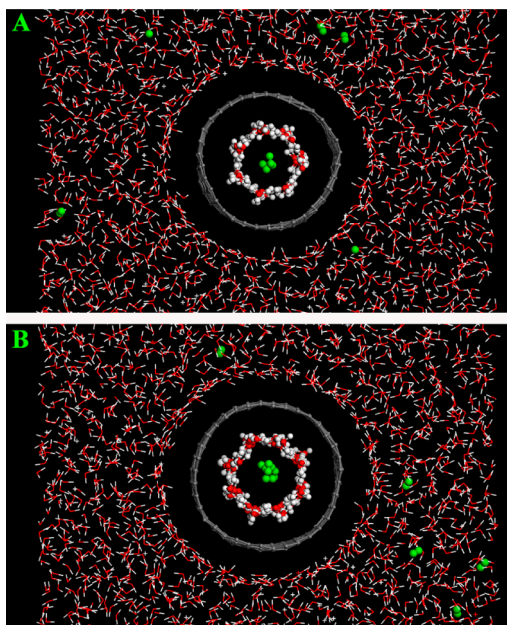

Figure 8. Snapshots of (A) heptagonal [at 250 K and 1 atm, in flexible (17,0) SW-CNT] and (B) octagonal [at 220 K and 1 atm, in flexible (18,0) SW-CNT] H_2 hydrates formed inside finite-size SW-CNTs. The SW-CNTs are always immersed in a water–H_2 solution where the H_2O/H_2 ratio is approximately 188:1.

or liquid-like molecule wire. If confirmed in the laboratory, these new forms of Q1D H_2 hydrates not only will enrich the gas-hydrate family, but also may offer a clean and safe way to store large-quantity hydrogen near the ambient condition. Although the gravimetric density of Q1D hexagonal H_2

hydrates is relatively low for automobile applications, the hydrates can provide a very safe way for on-demand hydrogen release without separation issues (for example, carbon-monoxide free) for portable electronic device applications.

■ ASSOCIATED CONTENT

Ⓢ Supporting Information

Classical MD simulations with the Silvera-Goldman (exp-6-8-10) potential for H_2–H_2 and H_2–C interactions; the structures formed by changing the number of water and H_2 molecules; the axial density profiles in hydrates; *NPT* classical MD simulations of finite-size SW-CNTs immersed in water-H_2 mixture; and movies of classical MD and AIMD trajectories of Q1D H_2 gas hydrates confined in SW-CNTs. This material is available free of charge via the Internet at http://pubs.acs.org.

■ AUTHOR INFORMATION

Corresponding Authors
francisc@purdue.edu
xzeng1@unl.edu

Author Contributions
[#]These authors contribute equally to this work.

Notes
The authors declare no competing financial interest.

■ ACKNOWLEDGMENTS

■ REFERENCES

(1) Sloan, E. D.; Koh, C. *Clathrate Hydrates of Natural Gases*; CRC Press: Boca Raton, FL, 2007.

(2) Koh, C. A.; Sloan, E. D.; Sum, A. K.; Wu, D. T. *Annu. Rev. Chem. Biomol. Eng.* **2011**, *2*, 237−257.

(3) Mao, W. L.; Mao, H.-k.; Goncharov, A. F.; Struzhkin, V. V.; Guo, Q.; Hu, J.; Shu, J.; Hemley, R. J.; Somayazulu, M.; Zhao, Y. *Science* **2002**, *297*, 2247−2249.

(4) Patchkovskii, S.; Tse, J. S. *Proc. Natl. Acad. Sci. U.S.A.* **2003**, *100*, 14645−14650.

(5) Mao, W. L.; Mao, H. *Proc. Natl. Acad. Sci. U.S.A.* **2004**, *101*, 708−710.

(6) Lee, H.; Lee, J.-w.; Kim, D. Y.; Park, J.; Seo, Y.-T.; Zeng, H.; Moudrakovski, I. L.; Ratcliffe, C. I.; Ripmeester, J. A. *Nature* **2005**, *434*, 743−746.

(7) Struzhkin, V. V.; Militzer, B.; Mao, W. L.; Mao, H.; Hemley, R. J. *Chem. Rev.* **2007**, *107*, 4133−4151.

(8) Hakim, L.; Koga, K.; Tanaka, H. *Phys. Rev. Lett.* **2010**, *104*, 115701.

(9) Smirnov, G. S. *J. Phys. Chem. Lett.* **2013**, *4*, 3560−3564.

(10) Florusse, L. J.; Peters, C. J.; Schoonman, J.; Hester, K. C.; Koh, C. A.; Dec, S. F.; March, K. N.; Sloan, E. D. *Science* **2004**, *306*, 469−471.

(11) Chapoy, A.; Anderson, R.; Tohidi, B. *J. Am. Chem. Soc.* **2007**, *129*, 746−747.

(12) Prasad, P. S. R.; Sugahara, T.; Sum, A. K.; Sloan, E. D.; Koh, C. A. *J. Phys. Chem. A* **2009**, *113*, 6540−6543.

(13) Sugahara, T.; Haag, J. C.; Prasad, P. S. R.; Warntjes, A. A.; Sloan, E. D.; Sum, A. K.; Koh, C. A. *J. Am. Chem. Soc.* **2009**, *131*, 14616−14617.

(14) Vos, W. L.; Funger, L. W.; Hemley, R. J.; Mao, H. *Phys. Rev. Lett.* **1993**, *71*, 3150−3153.

(15) Duarte, A. R. C.; Shariati, A.; Rovetto, L. J.; Peters, C. J. *J. Phys. Chem. B* **2008**, *112*, 1888−1889.

(16) Alavi, S.; Ripmeester, J. A. *Angew. Chem., Int. Ed.* **2007**, *46*, 6102−6105.

(17) Hakim, L.; Koga, K.; Tanaka, H. *Phys. Rev. B* **2010**, *82*, 144105.

(18) Hirai, H.; Kagawa, S.; Tanaka, T.; Matsuoka, T.; Yagi, T.; Ohishi, Y.; Nakano, S.; Tamamoto, Y.; Irifune, T. *J. Chem. Phys.* **2012**, *137*, 074505.

(19) Koh, D.-Y.; Kang, H.; Jeon, J.; Ahn, Y.-H.; Park, Y.; Kim, H.; Lee, H. *J. Phys. Chem. C* **2014**, *118*, 3324−3330.

(20) Plattner, N.; Meuwly, M. *J. Chem. Phys.* **2014**, *140*, 024311.

(21) Walsh, M. R.; Koh, C. A.; Sloan, E. D.; Sum, A. K.; Wu, D. T. *Science* **2009**, *326*, 1095−1098.

(22) (a) Koga, K.; Zeng, X. C.; Tanaka, H. *Phys. Rev. Lett.* **1997**, *79*, 5262−5265. (b) Bai, J.; Zeng, X. C.; Koga, K.; Tanaka, H. *Molecular Simulation* **2003**, *29*, 619−626. (c) Kaneko, T.; Bai, J.; Yasuoka, K.; Mitsutake, A.; Zeng, X. C. *J. Chem. Theory Comput.* **2013**, *9*, 3299−3310. (d) Kaneko, T.; Bai, J.; Yasuoka, K.; Mitsutake, A.; Zeng, X. C. *J. Chem. Phys.* **2014**, *140*, 184507.

(23) Zangi, R.; Mark, A. E. *J. Chem. Phys.* **2003**, *119*, 1694−1700.

(24) (a) Kumar, P.; Buldyrev, S. V.; Starr, F. W.; Giovambattista, N.; Stanley, H. E. *Phys. Rev. E* **2005**, *72*, 051503. (b) Giovambattista, N.; Rossky, P. J.; Debenedetti, P. G. *Phys. Rev. Lett.* **2009**, *102*, 050603.

(25) (a) Koga, K.; Gao, G. T.; Tanaka, H.; Zeng, X. C. *Physica A* **2002**, *314*, 462. (b) Bai, J.; Wang, J.; Zeng, X. C. *Proc. Natl. Acad. Sci. USA* **2006**, *103*, 19664−19667.

(26) Johnston, J. C.; Kastelowitz, N.; Molinero, V. *J. Chem. Phys.* **2010**, *133*, 154516.

(27) Han, S.; Choi, M. Y.; Kumar, P.; Stanley, H. E. *Nat. Phys.* **2010**, *6*, 685−689.

(28) Zhao, W.-H.; Bai, J.; Yuan, L.-F.; Yang, J.; Zeng, X. C. *Chem. Sci.* **2014**, *5*, 1757−1764.

(29) Bai, J.; Angell, C. A.; Zeng, X. C. *Proc. Natl. Acad. Sci. U.S.A.* **2010**, *107*, 5718−5722.

(30) Bai, J.; Zeng, X. C. *Proc. Natl. Acad. Sci. U.S.A.* **2012**, *109*, 21240−21245.

(31) Tanaka, H.; Koga, K. *J. Chem. Phys.* **2005**, *123*, 094706.

(32) Hummer, G.; Rasaiah, J. C.; Noworyta, J. P. *Nature* **2001**, *414*, 188−190.

(33) Koga, K.; Gao, G. T.; Tanaka, H.; Zeng, X. C. *Nature* **2001**, *412*, 802−805.

(34) Maniwa, Y.; Matsuda, K.; Kyakuno, H.; Ogasawara, S.; Hibi, T.; Kadowaki, H.; Suzuki, S.; Achiba, Y.; Kataura, H. *Nat. Mater.* **2007**, *6*, 135−141.

(35) Byl, O.; Liu, J.-C.; Wang, Y.; Yim, W.-L.; Johnson, J. K.; Yates, J. T. *J. Am. Chem. Soc.* **2006**, *128*, 12090−12097.

(36) Luo, C.; Fa, W.; Zhou, J.; Dong, J.; Zeng, X. C. *Nano Lett.* **2008**, *8*, 2607.

(37) Hess, B.; Kutzner, C.; van der Spoel, D.; Lindahl, E. *J. Chem. Theory Comput.* **2008**, *4*, 435−447.

(38) Zhao, W.-H.; Shang, B.; Du, S. P.; Yuan, L.-F.; Yang, J.; Zeng, X. C. *J. Chem. Phys.* **2012**, *137*, 034501.

(39) Jorgensen, W. J.; Chandrasekhar, J. D.; Madura, J. D.; Impey, R. W.; Klein, M. L. *J. Chem. Phys.* **1983**, *79*, 926.

(40) Cracknell, R. F. *Phys. Chem. Chem. Phys.* **2001**, *3*, 2091−2097.

(41) Silvera, I. F.; Goldman, V. V. *J. Chem. Phys.* **1978**, *69*, 4209−4213.

(42) Sun, D. Y.; Liu, J. W.; Gong, X. G.; Liu, Z.-F. *Phys. Rev. B* **2007**, *75*, 075424.

(43) Chen, H. Y.; Sun, D. Y.; Gong, X. G.; Liu, Z.-F. *Angew. Chem., Int. Ed.* **2013**, *52*, 1973−1976.

(44) Bussi, G.; Donadio, D.; Parrinello, M. *J. Chem. Phys.* **2007**, *126*, 014101.

(45) VandeVondele, J.; Krack, M.; Mohamed, F.; Parrinello, M.; Chassaing, T.; Hutter, J. *Comput. Phys. Commun.* **2005**, *167*, 103−128.

(46) Goedecker, S.; Teter, M.; Hutter, J. *Phys. Rev. B* **1996**, *54*, 1703.

(47) Hartwigsen, C.; Goedecker, S.; Hutter, J. *Phys. Rev. B* **1998**, *58*, 3641.

(48) Becke, A. D. *Phys. Rev. A* **1988**, *38*, 3098.

(49) Lee, C.; Yang, W.; Parr, R. G. *Phys. Rev. B* **1988**, *37*, 785.

(50) Grimme, S.; Antony, J.; Ehrlich, S.; Krieg, H. *J. Chem. Phys.* **2010**, *132*, 154104.

(51) Hujo, W.; Grimme, S. *Phys. Chem. Chem. Phys.* **2011**, *13*, 13942−13950.

(52) Mareš, J.; Liimatainen, H.; Laasonen, K.; Vaara, J. *J. Chem. Theory Comput.* **2011**, *7*, 2937−2946.

(53) Zhao, Y.; Li, H.; Zeng, X. C. *J. Am. Chem. Soc.* **2013**, *135*, 15549−15558.

(54) Martiniano, H. F. M. C.; Galamba, N.; Cabral, B. J. C. *J. Chem. Phys.* **2014**, *140*, 164511.

(55) Perdew, J. P.; Burke, K.; Ernzerhof, M. *Phys. Rev. Lett.* **1996**, *77*, 3865.

(56) Kolesnikov, A. I.; Zabotti, J.-M.; Loong, C.-K.; Thiyagarajan, P.; Moravsky, A. P.; Loutfy, R. O.; Burnham, C. *J. Phys. Rev. Lett.* **2004**, *93*, 035503.